Nanoscale

PAPER

View Article Online
View Journal | View Issue

Cite this: *Nanoscale*, 2015, **7**, 6527

Targeting ferritin receptors for the selective delivery of imaging and therapeutic agents to breast cancer cells†

S. Geninatti Crich,* M. Cadenazzi, S. Lanzardo, L. Conti, R. Ruiu, D. Alberti, F. Cavallo, J. C. Cutrin and S. Aime

Received 16th January 2015,
Accepted 3rd March 2015

DOI: 10.1039/c5nr00352k

www.rsc.org/nanoscale

In this work the selective uptake of native horse spleen ferritin and apoferritin loaded with MRI contrast agents has been assessed in human breast cancer cells (MCF-7 and MDA-MB-231). The higher expression of L-ferritin receptors (SCARA5) led to an enhanced uptake in MCF-7 as shown in T_2 and T_1 weighted MR images, respectively. The high efficiency of ferritin internalization in MCF-7 has been exploited for the simultaneous delivery of curcumin, a natural therapeutic molecule endowed with antineoplastic and anti-inflammatory action, and the MRI contrast agent Gd-HPDO3A. This theranostic system is able to treat selectively breast cancer cells over-expressing ferritin receptors. By entrapping in apoferritin both Gd-HPDO3A and curcumin, it was possible to deliver a therapeutic dose of 167 μg ml^{-1} (as calculated by MRI) of this natural drug to MCF-7 cells, thus obtaining a significant reduction of cell proliferation.

Introduction

The incidence of breast cancer, the most common cancer in women and the second cause of cancer death in women worldwide,[1] is currently growing.[2] Three major therapeutic approaches are used today to treat breast cancer, namely, surgical removal, irradiation, and chemotherapy. Anticancer treatments are based on three main approaches: (I) classical chemotherapy, (II) hormone therapy (III) and the emerging and promising targeted therapy, where signalling pathways deregulated in primary breast tumours are specifically targeted. Breast cancer treatment is still challenging, as drugs in use have serious undesired effects, and drug resistance is common, underlying the need for new targeted therapies.[3] Accordingly, reduced adverse effects and better outcome were reported when targeted therapies were applied. Therefore, much attention is currently devoted, particularly in the field of nanotechnologies applied to medicine, to the targeting of precise alterations affecting the interactome, transcriptome, epigenome, and the receptome (a network of membrane transporters used by cancer cells), leading to the design of more specific tailored therapies. Recently, various systems, *e.g.*, micelles, liposomes, biodegradable biopolymers and other nanoparticles loaded with contrast agents (CAs), have been proposed to noninvasively assess the accumulation at the target site of conjugated or co-entrapped drugs, and to predict and monitor therapeutic responses.[4] This therapeutic and at the same time diagnostic (hereinafter referred to as "theranostic") approach appears to have a great potential in providing highly specialized, more potent and safer tools to treat cancer.[5] The use of endogenous nanosized biomolecules for targeted cancer therapy is an interesting strategy for achieving this goal. Indeed, these molecules are ideal for the development of drug-delivery platforms, thanks to their biocompatibility and biodegradability. There are several examples in the literature showing the potential of natural systems carrying CAs to detect diseases, some of them exploit the ferritin cavity.[6] Ferritin is the main iron storage protein and is composed of 24 subunits of heavy (H)- or light (L)-chain peptides that are present at different ratios in various organs to form a cage architecture 12 nm in external diameter with an interior cavity of 8 nm. Once deprived of iron, the inner cavity can be used as a universal drug-delivery platform.[7] Several groups have functionalized the protein cage with specific ligands such as peptides (*e.g.* RGD),[8] growth factors (*e.g.* EGF),[9] and biotin[10] to improve its targeting capability. Recently, it was reported that H-ferritin interacts with cells through the transferrin receptor[11] (TfR-1) and can be used to transport doxorubicin selectively to cancer cells overexpressing TfR-1.[12] Herein, HoS-apoferritin (horse spleen apoferritin, 85% and 15% L and H chains, respectively) is investigated for the simultaneous

University of Turin, Department of Molecular Biotechnology and Health Sciences, via Nizza 52, Torino, Italy. E-mail: simonetta.geninatti@unito.it; Fax: +39 011 6706487; Tel: +39 011 6706473

†Electronic supplementary information (ESI) available: Competition studies with free apoferritin, Fig. S1; APO-FITC intracellular distribution by immunofluorescence, Fig. S2. See DOI: 10.1039/c5nr00352k

delivery of therapeutic and imaging agents (loaded into its internal cavity) to breast cancer cells by exploiting the L-ferritin transporting route without any further chemical functionalization of the protein surface. In fact, although L-ferritin functions are traditionally associated with intracellular iron storage, additional functions related to iron delivery based on a transferrin-independent mechanism to different target organs such as the brain, liver and spleen have been recently discovered and investigated.[13] The involved receptors belong to scavenger receptor class A member 5 (SCARA5)[14] for L-ferritin and to TIM-2[15] and TfR-1[11] for H-ferritin, respectively.

The relationship between ferritin and cancer arises from studies demonstrating an increase of the total ferritin (rich in L-chains) in the serum of patients with various malignancies.[16] However, the evaluation of L-ferritin levels in tumour tissue itself has revealed a complex, disease-specific picture. In some cases such as colon cancer, testicular seminoma, and breast cancer, an increase in L-ferritin level in tumour *versus* normal tissue has been reported.[17] In other cases, including liver cancer, a decrease in L-ferritin level has been observed.[17] In breast cancer patients, the available data show that the ferritin increase correlates with disease stage and that elevated serum concentration may be associated with local release within the breast tumor microenvironment. Moreover, breast tumor lysates also show elevated levels of L-ferritin, the predominant subunit observed in serum, and this increase correlates with advanced histological grade and shorter survival.[18] In this study, L-ferritin selective internalization has been investigated in breast cancer cells by using MRI. Moreover, apoprotein (apoferritin), obtained on iron elimination from the cavity, was loaded with Mn ions or with Gd-based CAs and exploited for the simultaneous delivery of curcumin, a natural therapeutic molecule endowed with anti-neoplastic and anti-inflammatory action.[19] Curcumin demonstrates anti-cancer activities both *in vitro* and *in vivo* by diverse mechanisms. It hinders proliferation and induces apoptosis in a wide range of cancer cell types *in vitro*, including breast, bladder, lung and other tissues.[20] Although clinical trials have demonstrated the safety of curcumin even at high doses (12 g per day), the clinical advancement of this promising natural compound is hampered by its poor water solubility and short biological half-life. For these reasons, much attention has been devoted to curcumin nanoformulations (liposomes, micelles, and polymeric nanoparticles) developed to protect it from fast degradation in aqueous solutions.[21] It has already been reported by our group that the encapsulation of curcumin inside the apoferritin cavity significantly increases its stability and bioavailability while maintaining its therapeutic anti-inflammatory properties in the attenuation of thioacetamide-induced hepatitis.[22] Although MRI sensitivity is lower with respect to nuclear and optical imaging modalities, the high spatial resolution (<100 μm) of MRI provides detailed morphological and functional information, and the absence of ionizing radiation makes it safer than techniques based on the use of radioisotopes. The MRI signal is dependent on the longitudinal (T_1) and transverse (T_2) proton relaxation times of water and the endogenous contrast can be altered by the use of CA that decreases T_1 and T_2 of water protons in the tissues where they are distributed.[23] In a proton MR image there is a direct proportionality between the observed signal intensity enhancement and the concentration of the CA. Thus, these agents can be used to carry out indirect curcumin quantification upon their introduction into the apoferritin cavity.

The aim of this study was to evaluate ferritin uptake and the efficacy with which ferritin delivers antineoplastic compounds to cancer cells. For this purpose, two human breast cancer cell lines, both expressing SCARA5,[24] namely MDA-MB-231 and MCF-7, were used.

Results and discussion

Horse spleen ferritin uptake

This study started with the evaluation of the ability of MCF-7 and MDA-MB-231 cells to take up ferritin from the incubation media. For this purpose, horse spleen ferritin (HoS-ferritin) containing *ca.* 1000 iron atoms per protein was used without any further modification. The experimental protocol was based on the measurement of the amount of iron internalized by MCF-7 and MDA-MB-231 cells, 6 and 24 hours upon incubation in the ferritin containing media, at 37 °C and 5% CO_2. The amount of internalized ferritin has been extrapolated by the ICP-MS determination of the intracellular Fe content. After 6 h of incubation, differences between the two cell lines were evident (Fig. 1). The amount of iron internalized by MCF-7 was significantly higher than in MDA-MB-231 cells and increased with ferritin concentration showing a saturating behaviour. To demonstrate the uptake specificity, competition assays were carried out by pre-incubating for 1.5 h MCF-7 cells with free apoferritin. Then ferritin was added to the medium and after 6 hours of incubation the amount of Fe taken up by cells was measured by ICP-MS. The internalized ferritin decreased by about 40% when the concentration of apoferritin particles added to the culture medium was 7 and 15 fold excess (see ESI†).

Ferritin contains a superparamagnetic ferrihydrite ($5Fe_2O_3{\cdot}9H_2O$) crystal which accelerates the transverse NMR relaxation (R_2) of solvent water protons causing a negative contrast in the corresponding images.[25] In fact, the presence of ferritin within tissues influences the T_2-weighted MRI signal intensity of liver, spleen, and brain, the organs where ferritin concentration is highest.[26] The effect of ferritin on MRI T_2-contrast increases to the magnetic field strength. Fig. 2A shows the R_2 values of a HoS-ferritin solution ([Fe] = 100 mM, loading factor = 1000) measured at different magnetic fields. R_2 increased dramatically with the magnetic field strengths, showing an enhanced sensitivity at high fields. Fig. 2B presents the T_2-weighted MRI images of HoS-ferritin labelled MDA-MB-231 and MCF-7 cells (5 μM HoS-ferritin concentration in the incubation medium, 24 h of incubation time). After incubation, cells were washed, transferred into glass capillaries, and placed in agar phantom to acquire MR images at 7 T. Cells incubated in the same medium without adding

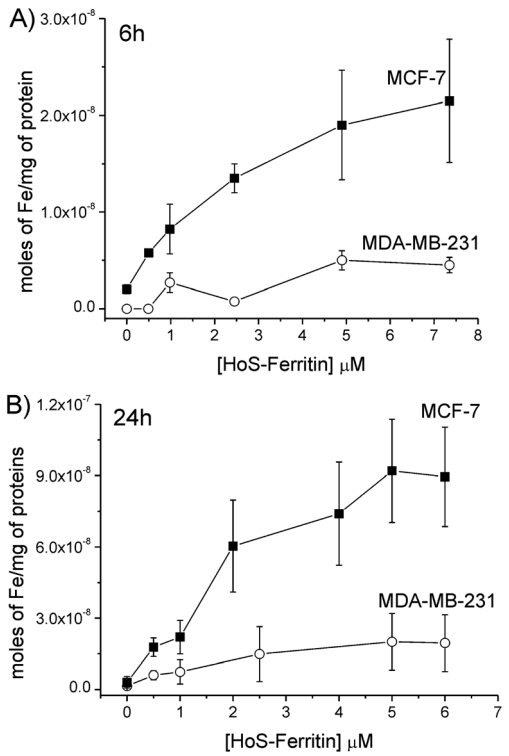

Fig. 1 Incubation of MDA-MB-231 (○) and MCF-7 (■) cells with HoS-ferritin for 6 h (A) and 24 h (B) at 37 °C. After incubation, cell lysates were analysed by ICP-MS to measure the amount of iron internalized by cells.

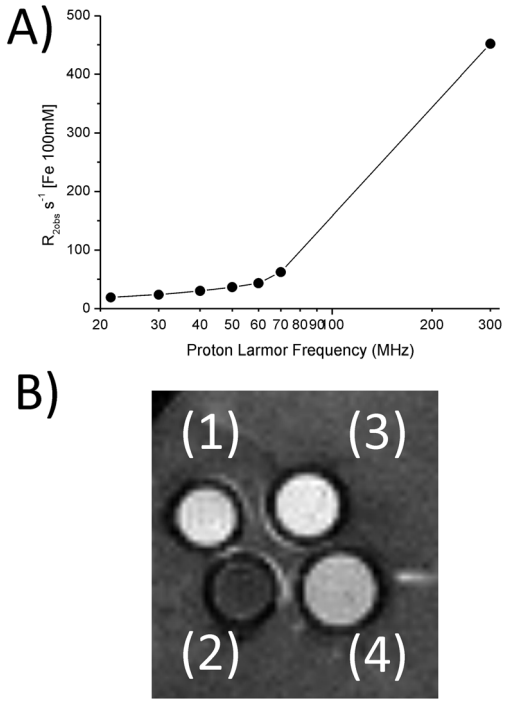

Fig. 2 (A) R_2 of native HoS-ferritin measured at different magnetic field strengths (T = 25 °C). (B) A representative T_2-weighted RARE MR image of agar phantoms containing (1) unlabeled MCF-7 cells; (2) MCF-7 incubated for 24 h with 5 μM HoS-ferritin; (3) unlabeled MDA-MB-231; (4) MDA-MB-231 incubated for 24 h with (5 μM) HoS-ferritin.

ferritin were used as a control. The T_2-weighted RARE (TR/TE/NEX = 5000/53/4) image confirms that the ferritin induced contrast is markedly more efficient in MCF-7 cells with respect to MDA-MB-231 (Fig. 2B). In fact, the signal intensity of MCF-7 cells incubated with ferritin is markedly lower than that observed in MDA-MB-231 cells due to the negative contrast generated by ferritin. As expected, it was not possible to detect any difference in T_1-weighted images of the same ferritin treated cells.

Since the negative contrast generated in MR images may be affected by a number of uncontrolled conditions associated with local inhomogeneities in the specimen and in the magnetic field, the longitudinal relaxation time (T_1) is considered the relaxation parameter that can be measured more accurately, and its value is less prone to get affected by uncontrolled experimental conditions. For this purpose the apoferritin cavity was loaded with positive CAs such as Mn ions or a commercially available Gd-complex. These molecules, characterized by a low R_2/R_1 ratio, are able to shorten T_1 and the consequence is that cells where they are entrapped appear brighter in a T_1 weighted image. Mn loaded apoferritin (Mn-Apo) is a highly sensitive MRI CA consisting of *ca.* 1000 manganese atoms entrapped in the inner cavity of apoferritin. The preparation of Mn-Apo was carried out following the reported procedure[27] based on the dissolution of the previously formed β-MnOOH inorganic phase performed *via* the reduction of Mn(III) to Mn(II) operated by aminopolycarboxylic acids that also act as sequestering agents for the weakly coordinated manganese ions on the outer surface of the protein (Fig. 3). The reductive treatment led to the attainment of a MRI agent endowed with a remarkably high relaxivity value (per apoferritin) of about 7000 mM^{-1} s^{-1}.

Cellular labelling experiments proved that, after 24 hours of incubation in the presence of Mn-Apo (0.075 μM protein concentration), the amount of internalized Mn was sufficient to generate hyperintense signals in MR images, recorded at 7 T, of MCF-7 cells (Fig. 4). The corresponding R_1 of MCF-7 increased proportionally with increasing the concentration of Mn-Apo added to the medium and reached a plateau at concentrations higher than 0.075 μM (Fig. 4). In contrast, for MDA-MB-231 the R_1 values were markedly lower and constant for the entire Mn-Apo concentration range considered (Fig. 4).

In order to prepare a theranostic system containing both a MRI CA and curcumin in the apoferritin cavity an alternative

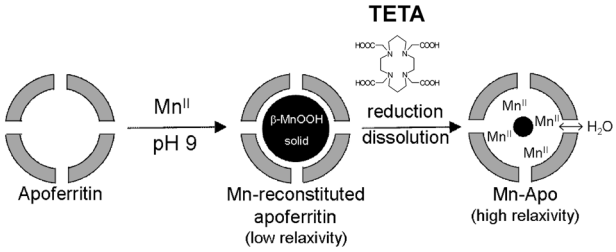

Fig. 3 Schematic representation of Mn-Apo preparation.

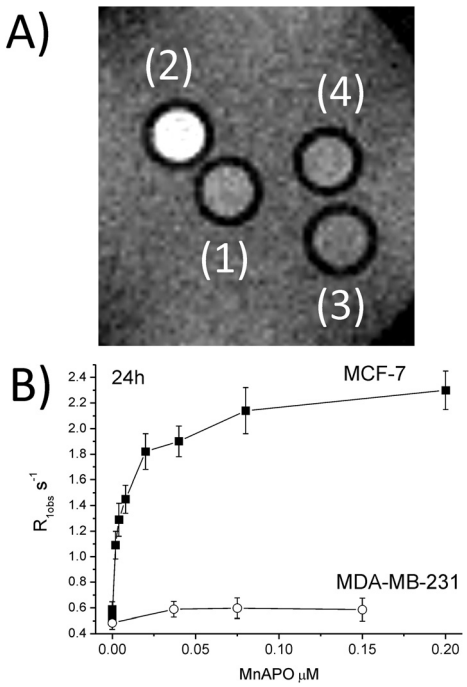

Fig. 4 (A) T_1-Weighted MRI image of agar phantoms containing (1) unlabeled MCF-7 cells; (2) MCF-7 incubated 24 h with (0.075 μM) Mn-Apo; (3) unlabeled MDA-MB-231; (4) MDA-MB-231 incubated with (0.075 μM) Mn-APO; (B) longitudinal relaxation rates (R_{1obs}) measured on MCF-7 and MDA-MB-231 cell pellets.

loading procedure[22] was carried out exchanging Mn^{2+} ions with a Gd-based commercially available CA (ProHance). It is a neutral Gd complex well tolerated by cells and organisms. The loading procedure consists in lowering the pH of the apoferritin containing solution, followed by the addition of the solutes to be uploaded.[28] The supramolecular structure of apoferritin collapses because of the rupture of the electrostatic interactions that maintain its spherical nanoarchitecture. When the pH is returned to 7 the spherical supramolecular shape of apoferritin (Gd-APO-CUR) is restored with the entrapment of the desired solutes in its inner cavity. The number of molecules that remained entrapped in apoferritin after the dissociation/reassociation procedure is 228 ± 48 and 9.6 ± 2 for curcumin and Gd-HPDO3A, respectively.

Fig. 5 shows the T_1 weighted MR image measured in MCF-7 and MDA-MB-231 cells incubated for 24 h at 37 °C in the presence of 1.3 and 2.7 μM Gd-APO-CUR. The differences between the two cell lines that were observed with native HoS-ferritin and Mn-Apo were reproduced also with this Gd-APO-CUR preparation. By measuring the R_1 of treated cells it was possible to calculate the intracellular Gd concentration by using the equation

$$[\mathrm{Gd}]\ \mathrm{mM} = (R_{1\mathrm{obs}} - R_{1\mathrm{d}})/r_{1\mathrm{p}}(\text{Gd-APO-CUR intra-cell}) \quad (1)$$

In eqn (1), R_{1obs} is the observed relaxation rate measured for each cell pellet at 7 T; R_{1d} is the diamagnetic contribution to the observed relaxation rate measured in untreated cells;

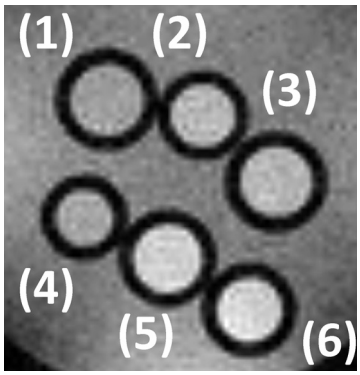

Fig. 5 T_1-Weighted MRI image of agar phantoms containing unlabeled MDA-MB-231 cells (1); MDA-MB-231 incubated for 24 h with 1.3 μM Gd-APO-CUR (2) and 2.7 (3) μM Gd-APO-CUR; unlabeled MCF-7 (4); MCF-7 incubated with 1.3 μM Gd-APO-CUR (5) and 2.7 (6) μM Gd-APO-CUR.

r_{1p} (Gd-APO-CUR intra-cell) is the intracellular millimolar relaxivity of the adduct (9.6 mM^{-1} s^{-1}). This value is significantly lower than that observed in water solution (r_{1p} = 17.7 mM^{-1} s^{-1}) as a consequence of the quenching effect due to the entrapment of the probe into endosomal/lysosomal vesicles.[29] This was confirmed by assessing the intracellular distribution of the apoferritin particles after 24 h of incubation with MCF-7 by immunofluorescence using FITC-labelled apoferritin (APO-FITC). Fig. S2 (ESI†) confirms that, at this time, most of the APO-FITC fluorescence was co-localized with lysosomes.

Since the curcumin/Gd ratio in the apoferritin preparation was 24, an estimated intracellular curcumin concentration of 167 μg ml^{-1} was obtained. In order to evaluate the cellular toxicity due to the presence of the Gd-HPDO3A complex in the theranostic probe, a batch of Gd-APO without curcumin was prepared using the same protocol reported above. Cell viability assessed using the trypan blue assay gave similar values of 88 ± 3, 89 ± 2 and 87 ± 3% for untreated cells and those treated with 1.3 μM and 2.7 μM Gd-APO, respectively.

SCARA5 detection

The observed difference in ferritin uptake by MCF-7 and MDA-MB-231 cells suggests a different expression of ferritin receptors in these breast cancer cell lines. In order to gain more insight into this issue, we examined the expression of the L-ferritin receptor SCARA5 by immunofluorescence. The cells were seeded on glass coverslips and allowed to adhere on this substrate overnight at 37 °C and 5% CO_2. The next day, coverslips were fixed and stained for SCARA5 expression and visualized with fluorescence microscopy. Although both cell lines expressed SCARA5, they did it with a different distribution as shown in Fig. 6. Whereas MCF-7 cells exhibited a diffuse plasma membrane fluorescence pattern, MDA-MB-231 presented a unique positive speckle (Fig. 6). This result is in line with that previously reported by Alkhateeb *et al.*[24] where the SCARA5 concentration, evaluated by the western blotting assay, was higher in MCF-7 with respect to MDA-MB-231.

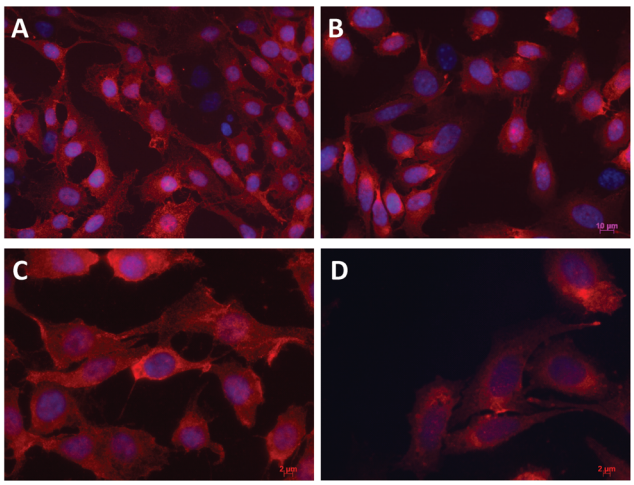

Fig. 6 SCARA5 staining of MCF-7 (A, C) and MDA-MB-231 (B, D) plated on glass coverslips. Cell nuclei were counterstained with DAPI. Images were acquired with an Apotome fluorescence microscope (Leica) of magnification ×20 (A, B) and ×100 (C, D).

Evaluation of curcumin and CUR-APO antiproliferative effect on MCF-7

In line with the results mentioned above, proliferation assays were performed only on MCF-7 highly expressing SCARA5 by incubating cells in the presence of APO-CUR, free apoferritin and free curcumin (added as 6.2 mg ml^{-1} DMSO solution) at two different concentrations (50 and 100 μM, respectively). The absence of long term toxic effects associated with the presence of DMSO in the culture media was verified incubating MCF-7 cells with the highest DMSO concentration used (0.6%) (Fig. 7). After incubation, cells were washed and the protein concentration was measured using the Bradford assay. Since the number of cells is proportional to the protein concentration, this value has been converted into the corresponding cell number using a previously obtained calibration curve. Fig. 7 shows that apoferritin alone did not affect cell proliferation as the obtained curve was similar to the control one. In contrast, the proliferation rate of cells incubated with 50 μM and 100 μM APO-CUR (curcumin concentration) is significantly lower compared with the control. As expected, the cytotoxic effect is proportional to the curcumin concentration and is similar to that observed by incubating curcumin alone at the same concentrations. Furthermore, from these results it is possible to confirm that the apoferritin cavity is able to protect curcumin from its degradation by maintaining its pharmacological properties also if dissolved in an aqueous medium, where usually it is fast degraded.

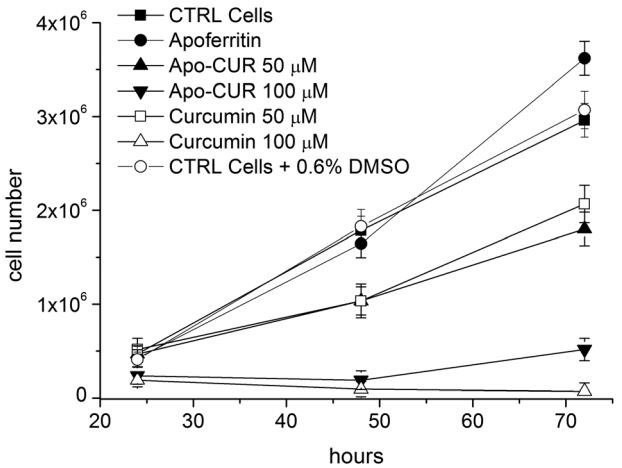

Fig. 7 Incubation of MCF-7 for 24 h with medium alone (■) or in the presence of: 0.6% DMSO (○), 0.5 μM apoferritin (●), 50 μM Apo-CUR (▲) and 100 (▼) μM Apo-CUR (curcumin concentration), and 50 μM curcumin alone (□) and 100 (△) μM curcumin alone for proliferation studies. Cell numbers have been calculated from the cell lysate protein concentration by using the Bradford assay (1 mg protein = 4.7 × 10^6 cells).

Conclusions

Apoferritin, without any further functionalization, can be proposed as a useful carrier of both therapeutics and imaging probes for MRI guided treatment of breast cancer cells characterized by up-regulation of ferritin uptake.

Furthermore, the access to the MRI approach can be exploited to gain a better understanding of the role of ferritin receptor expression in the evolution of the pathologies in which the accumulation and release of this protein are involved. Finally, immune-SCARA5 detection on breast cancer cells could be recommended for the detection of this therapeutic marker exploitable for a selective drug delivery.

Experimental

Gd-HPDO3A (ProHance) was kindly provided by Bracco Imaging S.p.A (Milan, Italy). Apoferritin, ferritin (from equine spleen), curcumin and all other chemicals were purchased from Sigma-Aldrich (St Louis, MO). Water proton T_1 and T_2 measurements were carried out on a Stelar SpinMaster spectrometer operating in the range 20–80 MHz by means of the inversion–recovery method (16 experiments, two scans) and a Carr Purcell Meiboom Gill Sequence (CPMG) for T_1 and T_2 measurements, respectively. The reproducibility of the T_1 data was ±0.5%. The final Fe, Gd and Mn concentrations were determined by inductively coupled plasma mass spectrometry (ICP-MS) (Element-2; Thermo-Finnigan, Rodano (MI), Italy). Sample digestion was performed with 2 ml of concentrated HNO_3 (70%) under microwave heating (Milestone MicroSYNTH Microwave Labstation).

Mn loaded apoferritin (Mn-Apo)

The Mn-Apo preparation was carried out as described previously.[27] Briefly, iron-free horse spleen apoferritin was reconstituted in the presence of $MnCl_2$ solution at pH = 9.0 under air. To avoid the fast oxidation of the Mn(II) ion, apoferritin

and Mn(II) were added into an N_2-saturated AMPSO [*N*-(1,1-dimethyl-2-hydroxyethyl)-3-amino-2-hydroxypropanesulfonic acid] solution, which had been previously corrected to the desired pH. The protein and the Mn(II) solutions were added to reach 1×10^{-6} and 3×10^{-3} M concentrations, respectively, corresponding to a loading of 3000 Mn(II) ions per apoferritin molecule. After 1 week reaction time, the samples were treated for 4 h at 20 °C with TETA (1,4,8,11-tetraazacyclotetradecane-1,4,8,11-tetraacetic acid) to reduce Mn(III) to Mn(II) as well as to remove Mn(II) ions bound to the outer surface of the protein shell. The obtained Mn-Apo solutions were characterized in terms of protein concentration by means of the Bradford method, using bovine serum albumin as a standard.

Gd-HPDO3A and curcumin loaded apoferritin (Gd-CUR-APO)

The loading of curcumin and Gd-HPDO3A in the iron free HoS-apoferritin cavity was carried out as described previously.[22] Briefly, the dissociation of the apoferritin into its subunits was done by lowering the pH of the 4.1×10^{-6} M protein solution (10 ml) to pH 2 using 1 M HCl and maintaining this low pH for about 15 min. Afterwards, 50 μL of a curcumin solution in DMSO (200 mg mL^{-1}) and 2 mL 0.5 M Gd-HPDO3A was added for every milliliter of apoferritin solution. Successively, the pH was adjusted to 7.4 using 1 M NaOH. The resulting solution was stirred at room temperature for 2 h and then, after centrifugation, purified by gel filtration (Superdex G25 Column, Amersham) and dialysis. The solution was then concentrated using Vivaspin centrifugal concentrators (50 000 MWCO). At the end of this process the concentrations of the protein (Bradford method), curcumin, and Gd were measured. The curcumin concentration has been measured spectrophotometrically at 430 nm in ethanol.

Cell lines

Human breast cancer cell lines (MDA-MB-231 and MCF-7) were obtained from ATCC. MDA-MB-231 cells were cultured in DMEM medium (Lonza) containing 10% (v/v) fetal bovine serum (FBS), 100 U ml^{-1} penicillin, 100 U ml^{-1} streptomycin, 0.01% plasmocin (InvivoGen) and 4 mM L-glutamine. MCF-7 cells were cultured in EMEM medium (Lonza) containing 10% (v/v) FBS, 100 U ml^{-1} penicillin and streptomycin, 1% (v/v) non-essential amino acid, 1 mM sodium pyruvate, 2 mM L-glutamine, and 0.01 mg ml^{-1} insulin. Cells were incubated at 37 °C under a humidified atmosphere of 5% CO_2. These cell lines were tested for mycoplasma (MycoAlert™ PLUS Mycoplasma Detection Kit, Lonza).

Uptake experiments

For HoS-ferritin, Mn-APO, APO-CUR, Gd-CUR-Apo and HoS-apoferritin uptake experiments MCF-7 and MDA-MB-231 were seeded at a density of 6×10^5 cells in a 25 cm^3 culture flask and placed in a wet (37 °C) 5% CO_2 air atmosphere incubator. For the different experiments, at 24 h post seeding, the cells were incubated with increasing concentrations of the above mentioned ferritin and apoferritins. After 6 or 24 h of incubation, cells were washed three times with 10 ml ice-cold PBS, detached with trypsin/EDTA. The Fe, Gd and Mn content in each cell line was determined by ICP-MS. For MRI analysis (see below) cells were transferred into glass capillaries. The protein concentration (proportional to the cell number) was determined from cell lysates by the Bradford assay, using bovine serum albumin as a standard.

MRI

All the MR images were acquired on a Bruker Avance 300 spectrometer (7 T) equipped with a Micro 2.5 microimaging probe (Bruker BioSpin, Ettlingen, Germany). *In vitro*: glass capillaries containing about 2×10^6 cells were placed in an agar phantom and MR imaging was performed by using a standard T_1-weighted multislice spin-echo sequence (TR/TE/NEX = 200/3.3/8 (Fig. 4) and TR/TE/NEX = 600/3.7/2 (Fig. 5), FOV = 1.2 cm, NEX = number of excitations; FOV = field of view). The T_1 relaxation times were calculated using a standard saturation recovery spin echo. T_2-Weighted MRI images were obtained using a RARE sequence protocol (TR/TE/NEX = 5000 : 43 : 2).

Proliferation assay

MCF-7 cells were seeded in a 25 cm^3 culture flask at a density of 2.5×10^5 cells. After 24 h, different concentrations of APO-CUR, free apoferritin, free curcumin dissolved in DMSO, or DMSO alone were added and at 24, 48 and 72 h post incubation, the media were removed and the cells were washed 3 times with 5 ml PBS. Cells were then treated with trypsin for 5 min at 37 °C, transferred into 15 ml falcon tubes, and centrifuged at 1100 rpm per 5 min. The supernatants were discarded and the cells were washed with PBS. At the end, cell pellets were resuspended in 200 μl PBS, sonicated, and protein concentrations were determined by the Bradford method. 1 mg of proteins correspond to 4.7×10^6 cells.

Scara5 detection

For Scara5 detection, 3×10^5 MCF-7 and MDA-MB-231 cells were plated on glass coverslips and left to adhere overnight at 37 °C in a 5% CO_2 incubator. Then, cells were fixed with 4% formalin solution in PBS (Sigma-Aldrich) for 10 min at room temperature and washed twice with PBS. Cells were then rinsed twice with PBS and non-specific binding was blocked with 10% bovine serum albumin (BSA, from Sigma-Aldrich) in PBS for 20 min at room temperature. Anti-SCARA5 antibody (Thermo Scientific™ Pierce™) was diluted 1/50 in PBS containing 1% BSA and added to the coverslips for 1 hour at room temperature. Cells were rinsed twice with PBS and then incubated with Alexa Texas Red-conjugated goat anti-rabbit (Life Technologies, 1/1000, and Molecular Probes, 1/1000) in PBS containing 1% BSA for 1 hour at room temperature. Cells were rinsed three times with PBS and air dried. Cell nuclei were counterstained with DAPI. Coverslips were mounted with Fluoromount mounting medium (Sigma-Aldrich) and visualized with an Apotome fluorescence microscope (Leica). Photographs were taken using a digital CCD camera and images were processed using the AxioVision (Zeiss, V. 4.4), Adobe

Photoshop and Microsoft PowerPoint software. The software program ImageJ was used to quantify fluorescence intensity.

Acknowledgements

This research was funded by MIUR (PRIN 2012 code 2012SK7ASN), by the AIRC Investigator Grant IG2013, by the University of Genova (Progetto San Paolo; title: Validazione di molecole per il rilascio tumore specifico di farmaci e la valutazione contestuale della risposta mediante imaging funzionale), and by Consorzio Interuniversitario di Ricerca in Chimica dei Metalli dei Sistemi Biologici (CIRCMSB). This research was performed in the framework of the EU COST Action TD1004. L.C. was supported by a fellowship from Fondazione Umberto Veronesi, under the "Pink is Good" project.

Notes and references

1 H. A. Azim and A. S. Ibrahim, *J. Thorac. Dis.*, 2014, **6**, 864–866; D. R. Youlden, *et al.*, *Cancer Biol. Med.*, 2014, **11**, 101–115.
2 C. Villareal-Graza, *et al.*, *Oncologist*, 2013, **18**, 1298–1306; E. de Azambuja, *et al.*, *Ann. Oncol.*, 2014, **25**, 525–528.
3 M. R. Stockler, *et al.*, *J. Clin. Oncol.*, 2011, **29**, 4498–4508; A. Dadla, *et al.*, *J. Oncol. Pharm. Pract*, 2014, Jul 5 (PMID: 24993705); A. H. Nwabu Kamaje, *et al.*, World, *J. Clin. Cases*, 2014, **2**, 769–786.
4 L. Y. Rizzo, B. Theek, G. Storm, F. Kiessling and T. Lammers, *Curr. Opin. Biotechnol.*, 2013, **24**, 1159–1166.
5 M. S. Muthu, D. T. Leong, L. Mei and S. S. Feng, *Theranostics*, 2014, **4**, 660–677; T. Lammers, S. Aime, W. E. Hennink, G. Storm and F. Kiessling, *Acc. Chem. Res.*, 2011, **44**, 1029–1038.
6 A. Maham, Z. Tang, H. Wu, J. Wang and Y. Lin, *Small*, 2009, **5**, 1706–1721.
7 Z. Zhen, W. Tang, T. Todd and J. Xie, *Expert Opin. Drug Delivery*, 2014, **11**, 1913–1922.
8 Z. Zhen, W. Tang, H. Chen, X. Lin, T. Todd, G. Wang, T. Cowger, X. Chen and J. Xie, *ACS Nano*, 2013, **7**, 4830–4837.
9 X. Li, L. Qiu, P. Zhu, X. Tao, T. Imanaka, J. Zhao, Y. Huang, Y. Tu and X. Cao, *Small*, 2012, **8**, 2505–2514.
10 H. Wu, J. Wang, Z. Wang, D. R. Fisher and Y. Lin, *J. Nanosci. Nanotechnol.*, 2008, **8**, 2316–2322; G. Liu, H. Wu, J. Wang and Y. Lin, *Small*, 2006, **2**, 1139–1143; S. Geninatti Crich, B. Bussolati, L. Tei, C. Grange, G. Esposito, S. Lanzardo, G. Camussi and S. Aime, *Cancer Res.*, 2006, **66**, 9196–9201.
11 L. Li, C. J. Fang, J. C. Ryan, E. C. Niemi, J. A. Lebrón, P. J. Björkman, H. Arase, F. M. Torti, S. V. Torti, M. C. Nakamura and W. E. Seaman, *Proc. Natl. Acad. Sci. U. S. A.*, 2010, **107**, 3505–3510.
12 M. A. Kilic, E. Ozlu and S. Calis, *J. Biomed. Nanotechnol.*, 2012, **8**, 508–514; M. Liang, K. Fan, M. Zhou, D. Duan, J. Zheng, D. Yang, J. Feng and X. Yan, *Proc. Natl. Acad. Sci. U. S. A.*, 2014, **111**, 14900–14905.
13 J. Fisher, K. Devraj, J. Ingram, B. Slagle-Webb, A. B. Madhankumar, X. Liu, M. Klinger, I. A. Simpson and J. R. Connor, *Am. J. Physiol. Cell Physiol.*, 2007, **293**, 641–649.
14 J. Y. Li, *et al.*, *J. Dev. Cell*, 2009, **16**, 35–46; M. B. Troadec, D. M. Ward and J. Kaplan, *Dev. Cell*, 2009, **16**, 3–4; J. Huang, D. L. Zheng, F. S. Qin, N. Cheng, H. Chen, B. B. Wan, Y. P. Wang, H. S. Xiao and Z. G. Han, *J. Clin. Invest.*, 2010, **120**, 223–241.
15 J. Han, W. E. Seaman, X. Di, W. Wang, M. Willingham, F. M. Torti and S. V. Torti, *PLoS One*, 2011, **6**, e23800, DOI: 10.137; B. Todorich, X. Zhang, B. Slagle-Webb, W. E. Seaman and J. R. Connor, *J. Neurochem.*, 2008, **107**, 1495–1505.
16 W. Wang, M. A. Knovich, L. G. Coffman, F. M. Torti and S. V. Torti, *Biochim. Biophys. Acta*, 2010, **1800**, 760–769.
17 A. A. Alkhateeb and J. R. Connor, *Biochim. Biophys. Acta*, 2013, **1836**, 245–254.
18 S. V. Chekhun, N. Y. Lukyanova, Y. V. Shvets, A. P. Burlaka and L. G. Buchynska, *Exp. Oncol.*, 2014, **36**(3), 179–183; I. Svitlana, *et al.*, *Breast Cancer Res. Treat.*, 2011, **126**, 63–71.
19 T. Esatbeyoglu, P. Huebbe, I. M. Ernst, D. Chin, A. E. Wagner and G. Rimbach, *Angew. Chem., Int. Ed.*, 2012, **51**, 5308–5332.
20 D. Liu and Z. Chen, *J. Breast Cancer*, 2013, **16**, 133–137; M. M. Yallapu, M. Jaggi and S. C. Chauhan, *Curr. Pharm. Des.*, 2013, **19**(11), 1994–2010.
21 O. Naksuriya, S. Okonogi, R. M. Schiffelers and W. E. Hennink, *Biomaterials*, 2014, **35**, 3365–3383; M. M. Yallapu, M. Jaggi and S. C. Chauhan, *Drug Discovery Today*, 2012, **17**, 71–80.
22 J. C. Cutrin, S. Geninatti Crich, D. Burghelea, W. Dastrù and S. Aime, *Mol. Pharm.*, 2013, **10**, 2079–2085.
23 P. A. Rinck, in *Magnetic Resonance in Medicine*, Blackwell Scientific Publications, Oxford, 2003.
24 A. A. Alkhateeb, B. Han and J. R. Connor, *Breast Cancer Res. Treat.*, 2013, **137**, 733–744.
25 Y. Gossuin, R. N. Muller and P. Gillis, *NMR Biomed.*, 2004, **17**, 427–432.
26 A. Hocq, M. Luhmer, S. Saussez, S. Louryan, P. Gillis and Y. Gossuin, *Contrast Media Mol. Imaging*, 2014, DOI: 10.1002/cmmi.1610; Y. Gossuin, R. N. Muller, P. Gillis and L. Bartel, *Magn. Reson. Imaging*, 2005, **23**, 1001–1004.
27 F. K. Kálmán, S. Geninatti Crich and S. Aime, *Angew. Chem., Int. Ed.*, 2010, **49**, 612–615; S. Geninatti Crich, J. C. Cutrin, S. Lanzardo, L. Conti, F. K. Kálmán, I. Szabó, N. R. Lago, A. Iolascon and S. Aime, *Contrast Media Mol. Imaging*, 2012, **7**, 281–288.
28 S. Aime, L. Frullano and S. Geninatti Crich, *Angew. Chem., Int. Ed.*, 2002, **41**, 1017–1019.
29 E. Terreno, S. Geninatti Crich, S. Belfiore, L. Biancone, C. Cabella, G. Esposito, A. D. Manazza and S. Aime, *Magn. Reson. Med.*, 2006, **55**, 491–497; M. B. Kok, S. Hak, W. J. Mulder, D. W. van der Schaft, G. J. Strijkers and K. Nicolay, *Magn. Reson. Med.*, 2009, **61**, 1022–1032.